International Journal of Scientific Engineering and Science
Volume 10, Issue 4, pp. 103-110, 2026. ISSN (Online): 2456-7361

Spectral Element Method for Second-Order Elliptic Interface Problems

Zhongrong Xiang[1], Lu Zhang[2], Rong Huang[3]
[1, 2, 3]School of Mathematical Sciences, Guizhou Normal University, Guiyang 550025, China
Email address: 3475614734@qq.com; [2]2976866162@qq.com; [3]1467221548@qq.com.

Abstract— *In this paper, we propose a Legendre-polynomial-based spectral element method for a class of one-dimensional second-order elliptic interface eigenvalue problems. First, a weak formulation of the original problem and its discrete counterpart are established. Then, the computational domain is partitioned into several subintervals according to the interface points. Within each subinterval, high-order Legendre polynomials are used to construct interior basis functions, while piecewise polynomial basis functions are introduced at the interfaces. This procedure yields a complete set of basis functions in the approximation space and allows the discrete formulation to be expressed in an equivalent matrix form. Extensive numerical experiments are conducted to verify the effectiveness of the proposed algorithm and to demonstrate its spectral accuracy.*

Keywords— *Spectral element method; interface eigenvalue problem; Legendre polynomials; Galerkin method.*

I. INTRODUCTION

As is well known, second-order elliptic interface problems form a fundamental class of partial differential equations, and their efficient numerical solution is crucial for simulations in a wide range of engineering and scientific applications. Significant progress has been made in both the theoretical analysis and numerical computation of these problems [1,2,3]. Existing numerical approaches are primarily based on the finite element method and the finite difference method [4, 5, 6]. In particular, a class of quadratic immersed finite element (IFE) spaces for second-order elliptic interface problems has been developed, enabling efficient solutions on structured meshes. This advancement has facilitated numerous applied studies, and related work can be found in [11, 12, 13, 14].

The finite element method is widely used in computational applications due to its flexibility [2, 7], whereas the spectral method is a high-order numerical technique known for its spectral accuracy [8, 9]. The spectral element method combines the spectral accuracy of the spectral method with the geometric flexibility of the finite element method, making it suitable for problems with complex boundaries and irregular domains [10]. However, applications of the spectral element method to one-dimensional second-order elliptic interface problems remain relatively limited. Motivated by this, the present paper develops an efficient spectral element method for one-dimensional second-order elliptic interface problems. First, by introducing appropriate Sobolev spaces based on the boundary conditions, we establish the weak formulation and its discrete scheme. Then, the construction of basis functions and the implementation details of the algorithm are presented. Finally, a series of numerical examples are provided to demonstrate the effectiveness and spectral accuracy of the proposed method.

The remainder of this paper is organized as follows. In Section 2, we introduce a class of Sobolev spaces and establish the variational formulation along with its corresponding discrete scheme. Section 3 presents a detailed construction of the basis functions in the approximation space and derives the equivalent matrix form of the discrete scheme. In Section 4, the effectiveness of the proposed algorithm is demonstrated through numerical examples. Section 5 concludes the paper.

2 Introduction

In this paper, we direct our focus to the subsequent second-order elliptic interface eigenvalue problem:

$$\begin{aligned} &-(\beta(x)\zeta'(x))' = \lambda\zeta(x), \quad x \in I, \\ &\zeta(-1) = 0, \quad \zeta(1) = 0, \\ &[\zeta]|_{x=\alpha_i} = 0, \quad [\beta\zeta']|_{x=\alpha_i} = 0, \quad i = 1,2, \end{aligned} \tag{2.1}$$

where the interval $I = (-1,1)$, β: $I \to R^+$ be a positive function defined piecewise by

$$\beta = \begin{cases} \beta_1(x), & x \in (-1, \alpha_1) \\ \beta_2(x), & x \in (\alpha_1, \alpha_2) \\ \beta_3(x), & x \in (\alpha_2, 1) \end{cases} \tag{2.2}$$

and

$$\zeta|_{x=\alpha_i} = \zeta|_{x=\alpha_i^+} - \zeta|_{x=\alpha_i^-} = 0, \ \beta\zeta'|_{x=\alpha_i} = \beta\zeta'|_{x=\alpha_i^+} - \beta\zeta'|_{x=\alpha_i^-} = 0. \tag{2.3}$$

Next, we establish the variational form of the equations (2.1) and their corresponding discrete formats. First, we introduce the following Sobolve space:

International Journal of Scientific Engineering and Science
Volume 10, Issue 4, pp. 103-110, 2026. ISSN (Online): 2456-7361

$$L^2(I) := \{\zeta : \int_I \zeta^2 dx < \infty\},$$

$$H_0^1(I) := \{\zeta : \zeta \in L^2(I), \zeta' \in L^2(I), \zeta(\pm 1) = 0\},$$

with the corresponding inner products and the norms:

$$(\zeta,\eta) = \int_I \zeta\eta dx, \ \|\zeta\| = (\zeta,\zeta)^{\frac{1}{2}},$$
$$(\zeta,\eta)_1 = \int_I \zeta\eta + \zeta'\eta' dx, \ \|\zeta\|_1 = (\zeta,\zeta)_1^{\frac{1}{2}}. \tag{2.4}$$

Then, the weak form of (2.1) is: Find $\zeta \in H_0^1(I)$, such that

$$a(\zeta,\nu) = \lambda b(\zeta,\nu), \quad \forall \nu \in H_0^1(I), \tag{2.5}$$

where

$$a(\zeta,\nu) = \int_I \beta(x)\zeta'\nu' dx, \quad b(\zeta,\nu) = \int_I \zeta\nu dx.$$

Let V_N be the approximate space of $H_0^1(I)$, then the discrete format corresponding to (2.5) is: find $\zeta_N \in V_N$, such that:

$$a(\zeta_N,\nu_N) = \lambda_N b(\zeta_N,\nu_N), \quad \forall \nu_N \in V_N. \tag{2.6}$$

II. Design and implementation of the algorithm

In this section, we shall describe how to efficiently solve(2.6). We start by constructing a set of basis functions of the approximation spaceV_N.

Let

$$\varphi_i(t) = L_i(t) - L_{i+2}(t), \ (i = 0,1,\cdots,N-2),$$

where $L_i(t)$ is a Legendre polynomial of degree i.

Set

$$\begin{cases} t_1 = \dfrac{2(x+1)}{\alpha_1+1} - 1, \quad \hat{\zeta}(t_1) = \zeta(x), \ x \in (-1,\alpha_1), \\ t_2 = \dfrac{2(x-\alpha_1)}{\alpha_2-\alpha_1} - 1, \hat{\zeta}(t_2) = \zeta(x), \ x \in (\alpha_1,\alpha_2), \\ t_3 = \dfrac{2(x-\alpha_2)}{1-\alpha_2} - 1, \hat{\zeta}(t_3) = \zeta(x), \ x \in (\alpha_2,1). \end{cases}$$

We define the following internal basis functions:

$$\phi_{1,i}(x) = \begin{cases} \varphi_i(t_1(x)), & x \in (-1,\alpha_1), \\ 0, & others, \end{cases} \quad \phi_{2,i}(x) = \begin{cases} \varphi_i(t_2(x)), & x \in (\alpha_1,\alpha_2), \\ 0, & others, \end{cases}$$

$$\phi_{3,i}(x) = \begin{cases} \phi_i(t_3(x)), & x \in (\alpha_2,1), \\ 0, & others, \end{cases}$$

where $i = 0,1,\cdots,N-2$.

Let us further define the interface basis functions:

$$\psi_1 = \begin{cases} \dfrac{1+t_1(x)}{2}, & x \in (-1,\alpha_1), \\ \dfrac{1-t_2(x)}{2}, & x \in (\alpha_1,\alpha_2), \\ 0, & x \in (\alpha_2,1), \end{cases} \quad \psi_1 = \begin{cases} 0 & x \in (-1,\alpha_1), \\ \dfrac{1+t_2(x)}{2}, & x \in (\alpha_1,\alpha_2), \\ \dfrac{1-t_3(x)}{2}, & x \in (\alpha_2,1), \end{cases}$$

Without loss of generality, we assume that the interface points are $\alpha_1 = -0.3$ and $\alpha_2 = 0.5$. The graphs of the various basis functions and their derivatives are shown as follows:

International Journal of Scientific Engineering and Science
Volume 10, Issue 4, pp. 103-110, 2026. ISSN (Online): 2456-7361

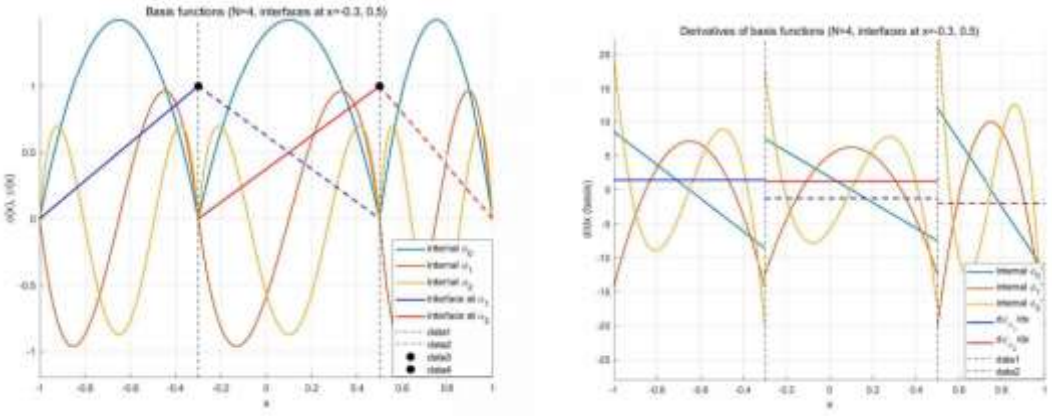

Figure 1: Figures of the basis functions with $N=4$ and $i = 0, 1, 2$.

It is obvious that

$$V_N = \bigcup_{j=1,2,3} \operatorname{span}\left\{\phi_{j,0}, \phi_{j,1}, \cdots, \phi_{j,N-2}\right\} \oplus \operatorname{span}\left\{\psi_1, \psi_2\right\}.$$

We expand ζ_N as follows:

$$\zeta_N = \hat{\xi}_{N-1}\psi_1 + \hat{\xi}_N\psi_2 + \sum_{i=0}^{N-2}\hat{\xi}_{1,i}\phi_{1,i} + \sum_{i=0}^{N-2}\hat{\xi}_{2,i}\phi_{2,i} + \sum_{i=0}^{N-2}\hat{\xi}_{3,i}\phi_{3,i}. \tag{3.1}$$

Substituting (3.1) into (2.6) and letting V_N run over a set of basis functions in V_N, equation (2.6) can be reduced to the following matrix form:

$$AU = \lambda_N BU,$$

where

$$A = \begin{bmatrix} A_1 & 0 & 0 & A_{1\alpha_1} & 0 \\ 0 & A_2 & 0 & A_{2\alpha_1} & A_{2\alpha_2} \\ 0 & 0 & A_3 & 0 & A_{3\alpha_2} \\ A_{1\alpha_1}{}^T & A_{2\alpha_1}{}^T & 0 & A_{\alpha_1\alpha_1} & A_{\alpha_1\alpha_2} \\ 0 & A_{2\alpha_2}{}^T & A_{3\alpha_2}{}^T & A_{\alpha_1\alpha_2}{}^T & A_{\alpha_2\alpha_2} \end{bmatrix}, B = \begin{bmatrix} B_1 & 0 & 0 & B_{1\alpha_1} & 0 \\ 0 & B_2 & 0 & B_{2\alpha_1} & B_{2\alpha_2} \\ 0 & 0 & B_3 & 0 & B_{3\alpha_2} \\ B_{1\alpha_1}{}^T & B_{2\alpha_1}{}^T & 0 & B_{\alpha_1\alpha_1} & B_{\alpha_1\alpha_2} \\ 0 & B_{2\alpha_2}{}^T & B_{3\alpha_2}{}^T & B_{\alpha_1\alpha_2}{}^T & B_{\alpha_2\alpha_2} \end{bmatrix}$$

$$U = \left[U_1, U_2, U_3, U_{\alpha_1}, U_{\alpha_2}\right]^T,$$

and

$$A_1 = (a_{ji}^1),\ A_{1\alpha_1} = (a_j^1),\ A_2 = (a_{ji}^2),\ A_{2\alpha_1} = (a_{j,N-1}^2),$$
$$A_{2\alpha_2} = (a_{j,N}^2),\ A_3 = (a_{ji}^3),\ A_{3\alpha_2} = (a_j^3),\ A_{\alpha_1\alpha_1} = (a^{11}),$$
$$A_{\alpha_1\alpha_2} = (a^{12}),\ A_{\alpha_2\alpha_2} = (a^{22}),\ B_1 = (b_{ji}^1),\ B_{1\alpha_1} = (b_j^1),$$
$$B_2 = (b_{ji}^2),\ B_{2\alpha_1} = (b_{j,N-1}^2),\ B_{2\alpha_2} = (b_{j,N}^2),\ B_3 = (b_{ji}^3),\ B_{3\alpha_2} = (b_j^3),$$
$$B_{\alpha_1\alpha_1} = (b^{11}),\ B_{\alpha_1\alpha_2} = (b^{12}),\ B_{\alpha_2\alpha_2} = (b^{22}),$$

$$U_1 = \left(\hat{\xi}_{1,0}, \hat{\xi}_{1,1}, \ldots, \hat{\xi}_{1,N-1}\right)^T, U_2 = \left(\hat{\xi}_{2,0}, \hat{\xi}_{2,1}, \ldots, \hat{\xi}_{2,N-1}\right)^T, U_3 = \left(\hat{\xi}_{3,0}, \hat{\xi}_{3,1}, \ldots, \hat{\xi}_{3,N-1}\right)^T,$$

and

International Journal of Scientific Engineering and Science
Volume 10, Issue 4, pp. 103-110, 2026. ISSN (Online): 2456-7361

$$a_{ji}^{1}=\int_{-1}^{1}\frac{2}{\alpha_1+1}(\beta(t_1))_1\varphi'_{1,i}\varphi'_{1,j}dt_1,\ a_{j}^{1}=\int_{-1}^{1}\frac{2}{\alpha_1+1}(\beta(t_1))_1\varphi'_{1,N-1}\varphi'_{1,j}dt_1,$$

$$a_{ji}^{2}=\int_{-1}^{1}\frac{2}{\alpha_2-\alpha_1}(\beta(t_2))_2\varphi'_{2,i}\varphi'_{2,j}dt_2,\ a_{j,N-1}^{2}=\int_{-1}^{1}\frac{2}{\alpha_2-\alpha_1}(\beta(t_2))_2\varphi'_{2,N-1}\varphi'_{2,j}dt_2,$$

$$a_{j,N}^{2}=\int_{-1}^{1}\frac{2}{\alpha_2-\alpha_1}(\beta(t_2))_2\varphi'_{2,N}\varphi'_{2,j}dt_2,$$

$$a_{ji}^{3}=\int_{-1}^{1}\frac{2}{1-\alpha_2}(\beta(t_3))_3\varphi'_{3,i}\varphi'_{3,j}dt_3,\ a_{j}^{3}=\int_{-1}^{1}\frac{2}{1-\alpha_2}(\beta(t_3))_3\varphi'_{3,N-1}\varphi'_{3,j}dt_3,$$

$$a^{11}=\int_{-1}^{1}\frac{2}{\alpha_1+1}(\beta(t_1))_1\varphi'_{1,N-1}\varphi'_{1,N-1}dt_1+\int_{-1}^{1}\frac{2}{\alpha_2-\alpha_1}(\beta(t_2))_2\varphi'_{2,N-1}\varphi'_{2,N-1}dt_2,$$

$$a^{12}=\int_{-1}^{1}\frac{2}{\alpha_2-\alpha_1}(\beta(t_2))_2\varphi'_{2,N}\varphi'_{2,N-1}dt_2,$$

$$a^{22}=\int_{-1}^{1}\frac{2}{\alpha_2-\alpha_1}(\beta(t_2))_2\varphi'_{2,N}\varphi'_{2,N}dt_2+\int_{-1}^{1}\frac{2}{1-\alpha_2}(\beta(t_3))_3\varphi'_{3,N-1}\varphi'_{3,N-1}dt_3,$$

$$b_{ji}^{1}=\int_{-1}^{1}\frac{\alpha_1+1}{2}\varphi_{1,i}\varphi_{1,j}dt_1,\ b_{j}^{1}=\int_{-1}^{1}\frac{\alpha_1+1}{2}\varphi_{1,N-1}\varphi_{1,j}dt_1,$$

$$b_{ji}^{2}=\int_{-1}^{1}\frac{\alpha_2-\alpha_1}{2}\varphi_{2,i}\varphi_{2,j}dt_2,\ b_{j,N-1}^{2}=\int_{-1}^{1}\frac{\alpha_2-\alpha_1}{2}\varphi_{2,N-1}\varphi_{2,j}dt_2,$$

$$b_{j,N}^{2}=\int_{-1}^{1}\frac{\alpha_2-\alpha_1}{2}\varphi_{2,N}\varphi_{2,j}dt_2,$$

$$b_{ji}^{3}=\int_{-1}^{1}\frac{1-\alpha_2}{2}\varphi_{3,i}\varphi_{3,j}dt_3,\ b_{j}^{3}=\int_{-1}^{1}\frac{1-\alpha_2}{2}\varphi_{3,N-1}\varphi_{3,j}dt_3,$$

$$b^{11}=\int_{-1}^{1}\frac{\alpha_1+1}{2}\varphi_{1,N-1}\varphi_{1,N-1}dt_1+\int_{-1}^{1}\frac{\alpha_2-\alpha_1}{2}\varphi_{2,N-1}\varphi_{2,N-1}dt_2,$$

$$b^{12}=\int_{-1}^{1}\frac{\alpha_2-\alpha_1}{2}\varphi_{2,N}\varphi_{2,N-1}dt_2,$$

$$b^{22}=\int_{-1}^{1}\frac{\alpha_2-\alpha_1}{2}\varphi_{2,N}\varphi_{2,N}dt_2+\int_{-1}^{1}\frac{1-\alpha_2}{2}\varphi_{3,N-1}\varphi_{3,N-1}dt_3,$$

where $i,j=0,1,2,\ldots,N-2$.

III. NUMERICAL EXPERIMENT

To demonstrate the convergence of the numerical eigenvalues with respect to N and to verify the high accuracy of the algorithm, we perform a series of numerical experiments using MATLAB 2024b.

Example 1: We set $\alpha_1=-0.5$ and $\alpha_2=0.6$. The coefficient β is taken to be constant on each subinterval:

$$\beta=\begin{cases}2, & x\in[-1,-0.5),\\ 3, & x\in(-0.5,0.6),\\ 5, & x\in(0.6,1].\end{cases}$$

Table 1 presents the numerical results of the first four eigenvalues, $\lambda_{Ni}, i=1,2,3,4$, for different values of N. Figure 2 shows the Figure of the reference solution and error plot between the reference solution at $N=100$ and the numerical solution at $N=40$. The convergence of the first four eigenvalues with respect to N is illustrated in Figure 3.

TABLE 1. Numerical results of the first four eigenvalues for different N.

N	λ_{N1}	λ_{N2}	λ_{N3}	λ_{N4}
5	7.263201238164	30.721529145	99	66.411281474	53	112.976658806	2
10	7.263201089354	30.721336625	61	66.382897247	38	112.489417893	3
20	7.263201089355	30.721336625	61	66.382897246	98	112.489417795	7
40	7.263201089350	30.721336625	60	66.382897246	96	112.489417795	7

International Journal of Scientific Engineering and Science
Volume 10, Issue 4, pp. 103-110, 2026. ISSN (Online): 2456-7361

As shown in Table 1, when $N \geq 20$, the first four numerical eigenvalues achieve a precision of at least 12 significant digits. Figure 2 illustrates the convergence of the eigenfunctions, showing that for $N \geq 40$ the numerical eigenfunctions reach a precision of approximately 10^{-14}. Furthermore, Figure 3 confirms the convergence and spectral accuracy of the first four eigenvalues.

Example 2: We set $\alpha_1 = -0.8$ and $\alpha_2 = 0$. The coefficient β is taken to be constant on each subinterval:

$$\beta = \begin{cases} 8, & x \in [-1, -0.8), \\ 12, & x \in (-0.8, 0), \\ 17, & x \in (0, 1]. \end{cases}$$

Table 2 presents the numerical results of the first four eigenvalues, $\lambda_{Ni}, i = 1,2,3,4$, for different values of N. Figure 4 shows the Figure of the reference solution and error plot between the reference solution at $N = 100$ and the numerical solution at $N = 40$. The convergence of the first four eigenvalues with respect to N is illustrated in Figure 5.

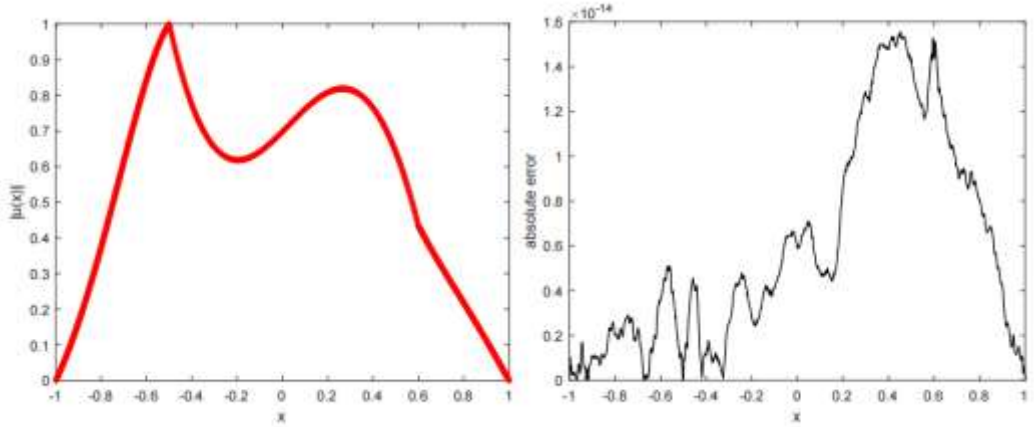

Figure 2:Figure of the reference eigenfunction with $N = 100$ (left) and the absolute error plot of the numerical eigenfunction with $N = 40$ (right).

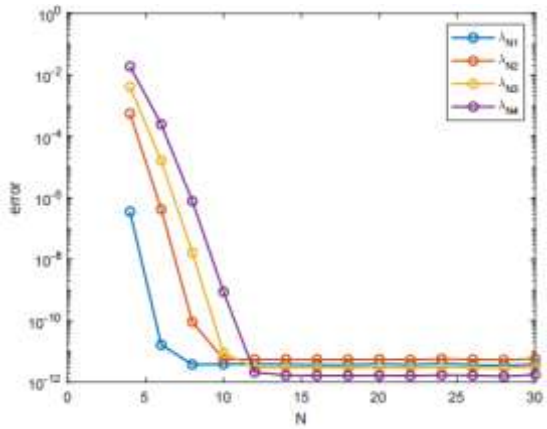

Figure 3: The error curves of the first four eigenvalues as N varies.

TABLE 2. Numerical results of the first four eigenvalues for different N.

N	λ_{N1}	λ_{N2}	λ_{N3}	λ_{N4}
5	3.241840037793	12.65798214447	30.10869581306	52.73226648263
10	3.241840031713	12.65795393859	30.10618201031	52.68774809735
20	3.241840031714	12.65795393859	30.10618201030	52.68774809467
40	3.241840031727	12.65795393859	30.10618201031	52.68774809467

As shown in Table 2, when $N \geq 20$, the first four numerical eigenvalues achieve a precision of at least 11 significant digits. Figure 4 illustrates the convergence of the eigenfunctions, showing that for $N \geq 40$ the numerical eigenfunctions reach a precision of approximately 10^{-14}. Furthermore, Figure 5 confirms the convergence and spectral accuracy of the first four eigenvalues.

International Journal of Scientific Engineering and Science
Volume 10, Issue 4, pp. 103-110, 2026. ISSN (Online): 2456-7361

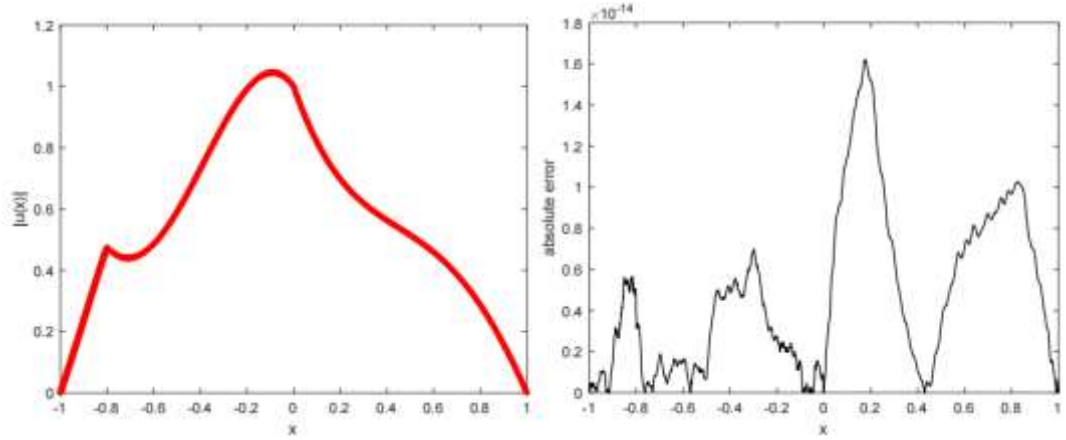

Figure 4: Figure of the reference eigenfunction with $N = 100$ (left) and the absolute error plot of the numerical eigenfunction with $N = 40$ (right).

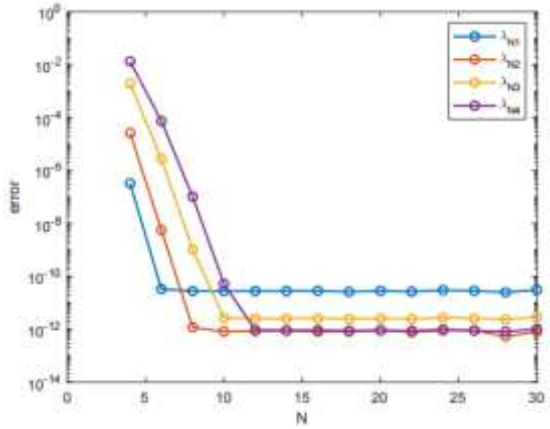

Figure 5: The error curves of the first four eigenvalues as N varies.

Example 3: We set $\alpha_1 = -0.8$ and $\alpha_2 = 0$. The coefficient β is taken to be constant on each subinterval:

$$\beta(x) = \begin{cases} 1+0.5\sin(\pi x), & x \in [-1,-0.8), \\ 1+0.5\cos(\pi x), & x \in (-0.8,0), \\ 1+0.5x^2, & x \in (0,1]. \end{cases}$$

Table 3 presents the numerical results of the first four eigenvalues, $\lambda_{Ni}, i = 1,2,3,4$, for different values of N. Figure 6 shows the Figure of the reference solution and error plot between the reference solution at $N = 100$ and the numerical solution at $N = 40$. The convergence of the first four eigenvalues with respect to N is illustrated in Figure 7.

TABLE 3. Numerical results of the first four eigenvalues for different N.

N	λ_{N1}	λ_{N2}	λ_{N3}	λ_{N4}
5	2.507188154339	11.17317250473	24.51851690222	43.62053900371
10	2.507174941562	11.17276669600	24.50356133806	43.52248147764
20	2.507174941511	11.17276669464	24.50356130407	43.52248116406
40	2.507174941511	11.17276669464	24.50356130407	43.52248116406

Again, as shown in Table 3, when $N \geq 20$, the first four numerical eigenvalues achieve a precision of at least 13 significant digits. Figure 6 illustrates the convergence of the eigenfunctions, showing that for $N \geq 40$ the numerical eigenfunctions reach a precision of approximately 10^{-14}. Furthermore, Figure 7 confirms the convergence and spectral accuracy of the first four eigenvalues.

International Journal of Scientific Engineering and Science
Volume 10, Issue 4, pp. 103-110, 2026. ISSN (Online): 2456-7361

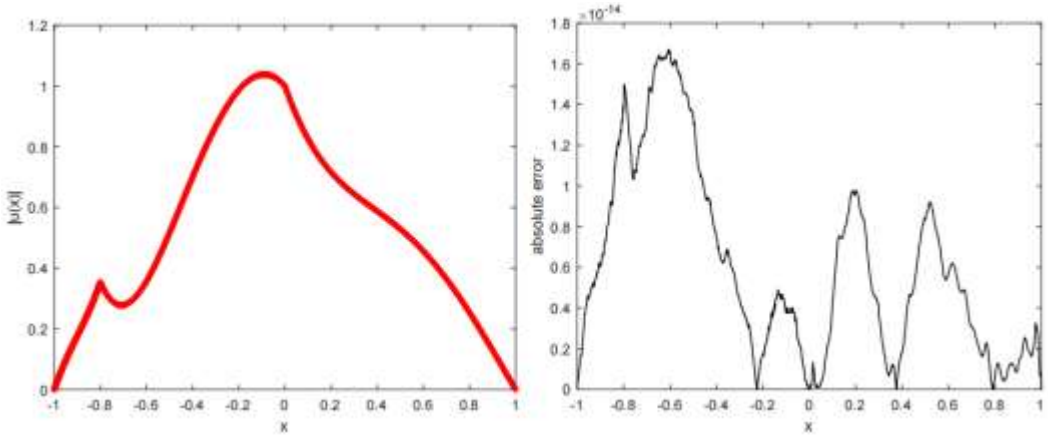

Figure 6: Figure of the reference eigenfunction with $N = 100$ (left) and the absolute error plot of the numerical eigenfunction with $N = 40$ (right).

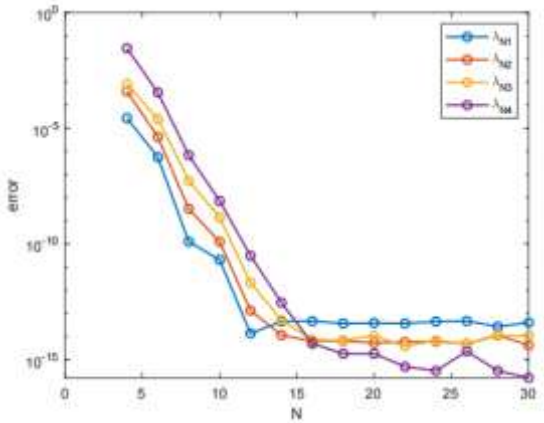

Figure 7: The error curves of the first four eigenvalues as N varies.

Example 4: We set $\alpha_1 = -0.6$ and $\alpha_2 = 0.5$. The coefficient β is taken to be constant on each subinterval:

$$\beta(x) = \begin{cases} 1 + 0.3e^{(-x^2)} + 0.2sin(\pi x), & x \in [-1, -0.6), \\ 1 + 0.2cos(2\pi x) + 0.1x^2, & x \in (-0.6, 0.5), \\ 1 + 0.4|x| + 0.2\sin(3x), & x \in (0.5, 1]. \end{cases}$$

Table 4 presents the numerical results of the first four eigenvalues, $\lambda_{Ni}, i = 1,2,3,4$, for different values of N. Figure 8 shows the Figure of the reference solution and error plot between the reference solution at $N = 100$ and the numerical solution at $N = 40$. The convergence of the first four eigenvalues with respect to N is illustrated in Figure 9.

TABLE 4. Numerical results of the first four eigenvalues for different N.

N	λ_{N1}	λ_{N2}	λ_{N3}	λ_{N4}
5	2.789481529699	11.53407421980	23.15426307286	42.05006264670
10	2.788110541433	11.52928180585	23.12851462096	41.99593080438
20	2.788110430426	11.52927639798	23.12848101902	41.99586721303
40	2.788110430426	11.52927639798	23.12848101901	41.99586721301

Finally, as shown in Table 4, when $N \geq 20$, the first four numerical eigenvalues achieve a precision of at least 12 significant digits. Figure 8 illustrates the convergence of the eigenfunctions, showing that for $N \geq 40$ the numerical eigenfunctions reach a precision of approximately 10^{-14}. Furthermore, Figure 9 confirms the convergence and spectral accuracy of the first four eigenvalues.

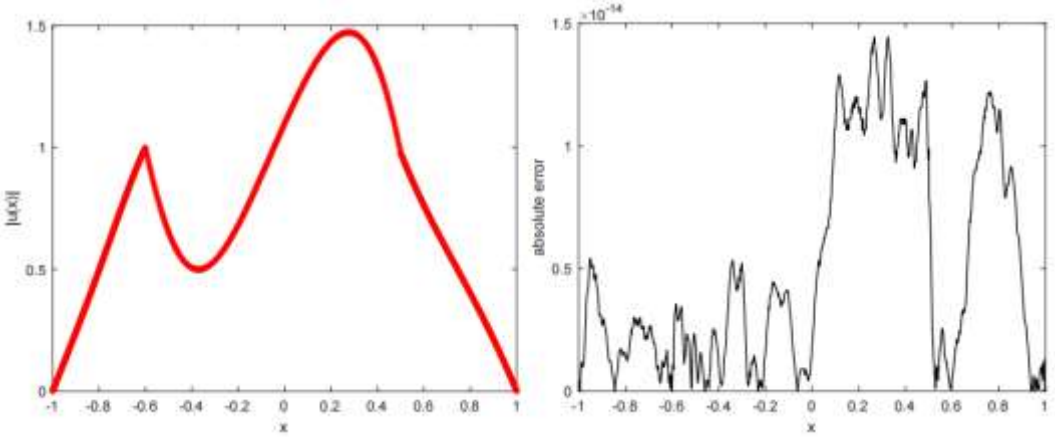

Figure 8: Figure of the reference eigenfunction with $N = 100$ (left) and the absolute error plot of the numerical eigenfunction with $N = 40$ (right).

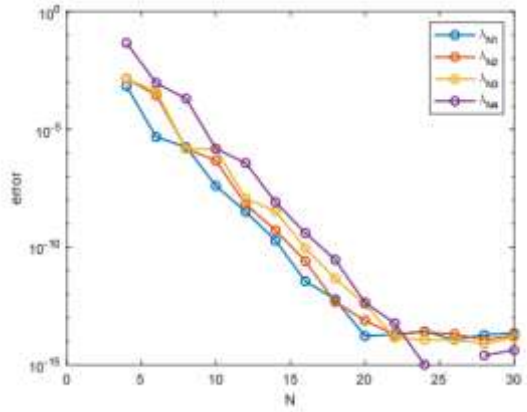

Figure 9: The error curves of the first four eigenvalues as N varies.

IV. Conclusions

In this work, we propose a spectral element method for solving one-dimensional second- order elliptic interface eigenvalue problems, which provides a high-order numerical scheme with spectral accuracy for interface problems involving piecewise smooth coefficients. This study not only offers new insights for interface problems on high-dimensional complex do- mains, but also lays a foundation for our future research objectives.

References

[1] Q. L. Wang, J. Liu, C. Y. Gong, et al. An efficient parallel algorithm for Caputo fractional reaction-diffusion equation with implicit finite-difference method. Advances in Difference Equations, 2016.
[2] L. Z. Chen, J. Shen, C. J. Xu. A Triangular Spectral Method for the Stokes Equations.Numerical Mathematics: Theory, Methods a nd Applications, 2011.
[3] Z. L. Lu, Y. P. Chen. L-error estimates of triangular mixed finite element methods for optimal control problems governed by semilinear elliptic equat ions. Numerical Analysis and Applications, 2009.
[4] Z. L. Li. The immersed interface method using a finite element formulation. Applied Numerical Mathematics, 1998.
[5] I. T. Angelova,L. G. Vulkov. High-order finite difference schemes for elliptic problems with intersecting interfaces. Applied Mathematics and Computation, 2007.
[6] H. Anita, H. Peter. An unfitted finite element method, based on Nitsches method, for elliptic interface problems. Computer Me thods in Applied Mechanics and Engineering, 2002.
[7] W. W. Zhu, G. H. Ji. A posteriori error estimates of the weak Galerkin finite element method for time-dependent Poisson-Nernst-Planck equations. Journal of Computa- tional and Applied Mathematics, 2026.
[8] J. Shen. Stable and Efficient Spectral Methods in Unbounded Domains Using Laguerre Functions. SIAM Journal on Numerical Analy sis, 2000.
[9] J. Shen, T. Tang. Spectral and High-Order Methods with Applications. Science Press, 2006.
[10] M. B. Hafeez, M. Krawczuk. A Review: Applications of the Spectral Finite Element Method. Archives of Computational Methods in Engineering, 2023.
[11] B. Camp, T. Lin, Y. Lin, W. Sun. Quadratic immersed finite element spaces and their approximation capabilities. Advances in C omputational Mathematics, 2006, 24(1).81- 112.
[12] T. Lin, Y. Lin, R. Rogers, L. Ryan. A rectangular immersed finite element space for interface problems. Adv. Comput. Theory Pract, 2001.
[13] S. Adjerid, I. Babus˘ka, R. Guo, et al. An enriched immersed finite element method for interface problems with nonhomogeneous jump conditions. Computer Methods in Applied Mechanics and Engineering, 2023, 404: 115770.
[14] S. H. Chou. An immersed linear finite element method with interface flux capturing recovery. Discrete & Continuous Dynamical Systems-Series B, 2012, 17(7).